Universal scalarization in topological AdS black holes

Zi-Qiang Zhao,[1] Zhang-Yu Nie,[2,*] Shao-Wen Wei,[3,†] Jing-Fei Zhang,[1] and Xin Zhang[1,4,5,‡]

[1] *Key Laboratory of Cosmology and Astrophysics (Liaoning), College of Sciences, Northeastern University, Shenyang 110819, China*

[2] *Center for Gravitation and Astrophysics, Kunming University of Science and Technology, Kunming 650500, China*

[3] *Lanzhou Center for Theoretical Physics, Key Laboratory of Theoretical Physics (Gansu) & Key Laboratory of Quantum Theory and Applications (MOE), Lanzhou University, Lanzhou 730000, China*

[4] *Key Laboratory of Data Analytics and Optimization for Smart Industry (Ministry of Education), Northeastern University, Shenyang 110819, China*

[5] *National Frontiers Science Center for Industrial Intelligence and Systems Optimization, Northeastern University, Shenyang 110819, China*

We investigate the universal behavior of black hole scalarization induced by a charged scalar field in the extended phase space of the asymptotic AdS spacetime with three distinct horizon topologies. The results indicate that in all the three cases, the charged black hole spacetime undergoes scalarization at low temperatures. Notably, the spherical topology is unique in that its domain of scalarization theoretically extends to much higher temperatures under low pressure in the extended phase space. Moreover, the scalarization process in the spherical case exhibits complex phase transition behaviors without additional non-linear terms, which are similar to those in the planar and hyperbolic topologies with the assistance of non-linear terms. With increasing pressure in the extended phase space, the condensate of the scalarization in all three cases undergoes a transition from the first-order style to a cave-of-wind style. This study provides deeper insight into the zeroth-order phase transition during black hole scalarization and reveals the complete phase structure of black holes in the extended phase space.

Introduction—Recent studies in gravitational theories have uncovered a remarkable phenomenon, spontaneous scalarization, which poses a novel challenge to the extensions of the no-hair theorem [1, 2]. Spontaneous scalarization is a phase transition in which compact objects develop a nontrivial scalar "hair" due to a tachyon instability. Initially identified in scalar-tensor theories for neutron stars [3], this phenomenon has since been extended to black holes. In extended scalar-tensor-Gauss–Bonnet (ESTGB) gravity [4–6], Schwarzschild black holes can undergo spontaneous scalarization, with curvature serving as the triggering mechanism. A similar effect occurs in Reissner–Nordström (RN) black holes within Einstein–Maxwell–scalar (EMS) models [7]. In certain ESTGB theories, Kerr black holes exhibit spin-induced scalarization [8]. Furthermore, a considerable number of analogous studies on scalarization have been conducted [9–12]. These scalarization mechanisms share a common feature: the general hairless solutions remain valid, but become unstable in certain regions of the parameter space, bifurcating into new families of scalarized black holes that are thermodynamically preferred. These hairy black holes generally exhibit richer phenomena.

The rich phase transition behavior of scalarized black holes in asymptotic AdS spacetime also provides a fruitful framework for investigating the AdS/CFT correspondence [13–20]. In a broader context, the cosmological constant can be treated as thermodynamic pressure within the extended phase space, leading to rich phase structures [21–26]. Scalarization in the extended phase space of the asymptotical AdS spacetime reveals the formation of scalarized black holes below a certain critical temperature as well as the zeroth order phase transition at a lower temperature [27, 28], which indicates the global instability of the system [29]. In a model with positive kinetic energy term and the potential term bounded from below, the system should be globally stable, which indicates that new solutions with lower thermodynamic potential are waiting for discovery. This leads to two fundamental questions: Do these new stable solutions really exist and what is the final phase diagram in the extended phase space of the black holes?

In this Letter, we investigate the spontaneous scalarization of topological AdS black holes, revealing a remarkable universality across different horizon geometries (spherical, planar, and hyperbolic). We consider a model where a charged scalar field with non-linear self-interactions couples to gravity. We demonstrate that scalarization occurs at low temperatures in all three topologies, with the spherical case exhibiting particularly intricate behavior—including cave-of-wind (COW) phase transitions and critical phenomena even in the absence of non-linear terms. Furthermore, we show that the pressure in the extended phase space universally drives the system from a zeroth-order to a first-order phase transition, and eventually to a supercritical region, in a manner analogous to the back-reaction parameter or non-linear term. A striking implication of our analysis is that in the low-pressure regime, all spherical AdS black holes may undergo a first-order transition into a scalarized state.

Model—There are various methods to induce spontaneous scalarization of black holes. In this Letter, we employ a charged scalar field model that includes one non-linear term. This model is also used in the study of holographic superconductors [14, 15, 29–31]. The non-linear term is introduced to generate zeroth-order phase transitions in planar and hyperbolic topologies, facilitating the study of universal properties. Spherical topology is special; it exhibits a zeroth-order phase transition without any higher-order non-linear term, a phenomenon also observed in uncharged scalar field [27]. The total action is

$$S = S_M + S_G \ , \quad S_G = \frac{1}{2\kappa_g^2}\int d^4x\sqrt{-g}\,(R-2\Lambda) \ ,$$
$$S_M = \frac{1}{q^2}\int d^4x\sqrt{-g}\Big(-\frac{1}{4}F_{\mu\nu}F^{\mu\nu} - D_\mu\psi^* D^\mu\psi - \frac{m^2}{L^2}\psi^*\psi - \lambda(\psi^*\psi)^2\Big) \ . \tag{1}$$

Here, $F_{\mu\nu} = \nabla_\mu A_\nu - \nabla_\nu A_\mu$ is the Maxwell field strength and $D_\mu\psi = \nabla_\mu\psi - iA_\mu\psi$ is the standard covariant derivative term of the charged scalar filed ψ. In which $\Lambda = -3/L^2$. Here L is the AdS radius, and in the black hole extended space L should be considered as the pressure of the black hole with $P = 3/(8\pi L^2)$.

The equations of motion for the matter fields are derived by varying the action with respect to the scalar and electromagnetic fields. We use the following ansatz

$$\psi = \psi(r) \ , \ A_\mu dx^\mu = \phi(r)dt \ . \tag{2}$$

We will discuss the universal laws we have discovered separately under spherical, planar, and hyperbolic topologies. The metric are as follows

$$ds^2 = -N(r)\sigma(r)^2dt^2 + \frac{1}{N(r)}dr^2 + r^2 d\Sigma_2^2 \ , \tag{3}$$

in which

$$N(r) = \frac{r^2}{L^2} - \frac{2M(r)}{r} + k \ , \tag{4}$$

where k = 1, 0 and -1 for spherical, planar, and hyperbolic topologies, respectively.

Given the metric and the Lagrangian, we can obtain the full equations of motion by solving the Einstein field equation. The Einstein filed equation is

$$R_{\mu\nu} - \frac{1}{2}(R-2\Lambda)g_{\mu\nu} = b^2\mathcal{T}_{\mu\nu}, \tag{5}$$

where $b = \kappa_g/q$ is the strength of back-reaction of matter fields on the background geometry and $\kappa_g^2 = 8\pi G$. $\mathcal{T}_{\mu\nu}$ is the stress-energy tensor of the matter fields

$$\mathcal{T}_{\mu\nu} =(-\frac{1}{4}F_{\alpha\beta}F^{\alpha\beta} - D_\alpha\psi^* D^\alpha\psi - \frac{m^2}{L^2}\psi^*\psi - \lambda(\psi^*\psi)^2)g_{\mu\nu} + (D_\mu\psi^* D_\nu\psi + D_\nu\psi^* D_\mu\psi) + F_{\mu\alpha}F_\nu^\alpha \ . \tag{6}$$

By solving the Einstein field equation, we can obtain the complete set of field equations encompassing both matter fields and the spacetime background. The Hawking temperature of these black hole metrics is

$$T = \frac{N'(r_h)\sigma(r_h)}{4\pi}, \tag{7}$$

where $r = r_h$ labels the radius of the event horizon.

By evaluating the on-shell action, we obtain the black hole's free energy. In this work, we consistently work within the canonical ensemble framework. The Gibbs free energy is

$$\widetilde{G} = -\frac{1}{\beta}ln\mathcal{Z} \ , \mathcal{Z} = e^{-S^E} \ , \tag{8}$$

where

$$S^E = -\frac{1}{2\kappa_g^2}\int d^4x\sqrt{-g}(R-2\Lambda+2b^2\mathcal{L}_M) + \frac{1}{\kappa_g^2}\int d^3x\sqrt{-h}\left(b^2 n_a F^{ab}A_b + K + \frac{2}{L} + \frac{2k}{r^2}\frac{L}{2}\right). \tag{9}$$

For simplicity and without loss of generality, we omit the spacetime integral constant, yielding the final form of the free energy as

$$G_k = \frac{2\kappa_g^2\widetilde{G_k}}{V_2}. \tag{10}$$

Universal phase structure—The black hole in an asymptotically planar AdS spacetime undergoes spontaneous scalarization when a charged scalar field is introduced. This occurs below a critical temperature T_c and leads to spontaneous symmetry breaking. Consequently, the black hole system acquires additional scalar hair, and the system's free energy becomes thermodynamic favor. However, when a negative higher-order non-linear term $\lambda(\psi^*\psi)^2$ is added, this scalarized solution is no longer stable, yet it still exists in a small stable region, known as the zeroth-order phase transition [19, 27, 29]. The size of this stable region depends on the value of the self-interaction parameter λ. This zeroth-order phase transition is progressively modified as the back-reaction parameter increases, gradually transitioning into a first-order phase transition, and ultimately entering the supercritical scalarized black hole region at a certain critical point. We have discussed this results in detail in Ref. [31]. This critical phenomenon is not unique to the back-reaction parameter. When focusing on pressure, we find that this critical phenomenon also persists.

In Fig. 1, we show the free energy as a function of temperature for the planar topology at different pressures, with corresponding landscape analysis. In this Letter, we do not compute the landscape exactly but

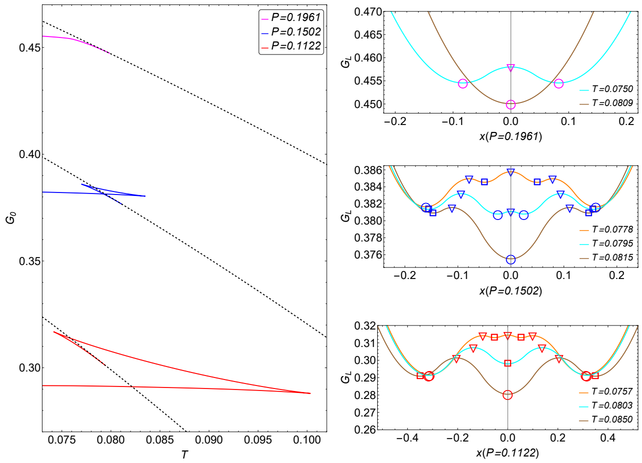

FIG. 1. The free energy and landscape. Left: The relationship between free energy and temperature for plane topology under different pressure, where the red solid line indicates a first-order phase transition, blue solid lines represent COW phase transitions, magenta solid lines denote second-order phase transitions, and black dashed lines is the normal solution. Right: Landscape analysis corresponding to different pressure on the right-hand side. Different colors represent different pressures. Circles denote stable states, squares represent metastable states, and inverted triangles indicate unstable states. The value of G_L corresponds to that of the conjectured landscape analysis, where only the extremal points satisfy the equations of motion.

rather provide its conjectured form based on the values of the free energy, which means only the extremal points satisfy the equations of motion. In Fig. 1, the red solid line corresponds to first-order phase transitions. With increasing pressure, it becomes the blue solid line indicating the COW phase transition, and eventually becomes the magenta solid line indicating supercritical scalarized black holes. Our analysis in Ref. [29] shows that zeroth-order phase transitions are unstable configurations, when there exists any additional higher-order non-linear term, no matter how small, the zeroth-order transition will always turn into a first-order phase transition when the scalar field becomes sufficiently large. Ref. [31] further demonstrates that the back-reaction parameter b has effects equivalent to higher-order non-linear terms. The results presented in Fig. 1 indicate that pressure also exhibits effects similar to higher-order non-linear terms, meaning that as long as the pressure is non-zero, all zeroth-order phase transitions will transform into first-order phase transitions at sufficiently high temperatures.

Figs. 2(a) and 2(b) show phase diagrams for planar topology under varying back-reaction and pressure respectively. The red solid line marks transition points between different scalarized black hole solutions in COW phase transitions. The red dashed line indicates the transition points of first-order phase transitions between normal and scalarized black holes. The blue dashed lines show the spinodal region of the COW and first-order phase transitions. All COW phase transitions terminate at a critical point before entering the supercritical regime. Fig. 2(c) presents the $P-T$ phase diagram for the hyperbolic topology, exhibiting the same transition behavior to the planar cases.

Scalarization in spherical topology— Let us now focus on the most interesting case: spherical topology. When $\psi = 0$ in the action (1), the metric (4) with $k = 1$ reduces to the familiar RN-AdS black hole. The only difference is that in our model, the metric of the RN-AdS black hole will have an additional back-reaction parameter b

$$N(r) = 1 + \frac{b^2 Q^2}{2r^2} + \frac{r^2}{L^2} - \frac{2M}{r} \,, \tag{11}$$

where the mass can be expressed with the radius of the black horizon

$$M = \frac{b^2 Q^2}{4 r_h} + \frac{r_h}{2} + \frac{r_h^3}{2L^2}. \tag{12}$$

In this subsection, we set $\lambda = 0$, implying that the system lacks non-linear terms. For computational convenience, we choose $b = 0.4$. We have also computed results for other values of b, with qualitatively similar behavior observed. At a low pressure, the system exhibits the familiar first-order phase transition in the extended phase space of the RN-AdS black hole, eventually reaching a critical point with increasing pressure, beyond which the system enters the supercritical regime. This result corresponds to the black solid line in Fig. 3(b), the red point is the critical point of RN-AdS black hole.

Numerical results indicate the existence of an unstable scalarized black hole solution with higher free energy for the black hole system at this stage. If we continue to increase pressure, we find that this unstable solution transitions into a small stable region, corresponding to the zeroth-order phase transition we are familiar with from planar and hyperbolic topologies. Theoretically, such an unstable phase transition model should not exist. An effective approach is to introduce an additional higher-order non-linear term. However, as we discussed earlier in this letter and in the previous study [31], both pressure and back-reaction parameters have similar effects to higher-order non-linear terms. Consequently, upon further increasing pressure, this unstable zeroth-order phase transition evolves into a first-order phase transition.

In Fig. 3(a), we show the phase transition behavior of scalarized black holes with increasing pressure. A metastable solution appears briefly at the unstable solution of zeroth-order phase transition and then evolves into a first-order phase transition between stable and metastable states. With a further increase in pressure, the unstable branch of the zeroth-order phase transition

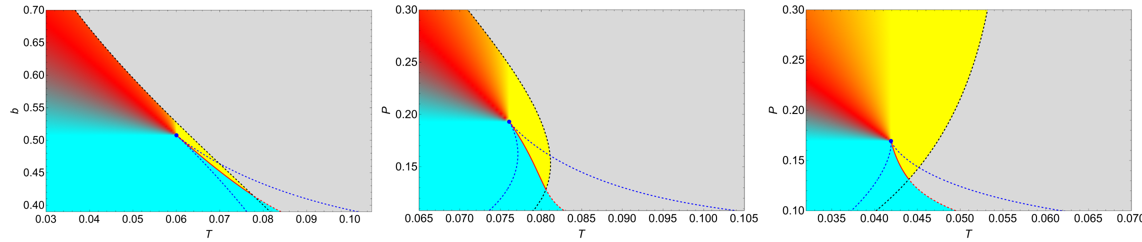

(a) (b) (c)

FIG. 2. The phase diagrams of planar and hyperbolic topologies. Panel (a): The phase diagram of $b-T$ for planar topology with fixed $L=1$ and $\lambda=-0.35$. Panel (b): The phase diagram of $P-T$ for planar topologies with fixed $b=0.4$ and $\lambda=-0.35$. Panel (c): The phase diagram of $P-T$ for hyperbolic topologies with fixed $b=0.4$ and $\lambda=-0.2$. The red solid and red dashed lines represent the COW and the first-order phase transitions. The blue dashed line delineates the spinodal regions for these phase transitions. The gray area signifies the normal solution, while the yellow and cyan regions correspond to two distinct hairy scalar solutions. The red region denotes the supercritical regime.

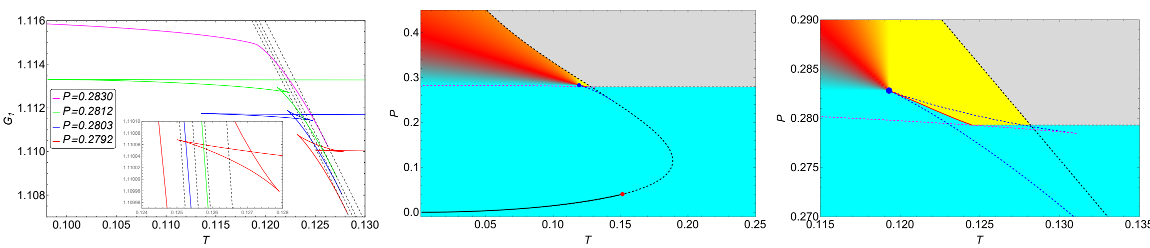

(a) (b) (c)

FIG. 3. The free energy and phase diagram for sphere topology with $\lambda=0$ and $b=0.4$. Panel (a): The black dashed and solid lines are for the normal and scalaried solutions. Panels (b) and (c): The phase diagram of sphere topology. The red region is the supercritical scalaried black hole region, the yellow and cyan region are the two different scalaried solution regions. Panel (c): The enlarged diagram of panel (b).

rapidly approaches zero temperature. The system then exhibits a standard first-order phase transition characterized by a swallowtail curve, eventually entering a supercritical region. This behavior is consistent with planar and hyperbolic topologies.

By calculating the free energy profiles across all pressure values, we obtain the phase diagram for scalarized black holes with spherical topology. Fig. 3(b) shows the complete phase diagram, while Fig. 3(c) provides a magnified view.

As previously analyzed, the spherical topology exhibits the same phase structure as planar and hyperbolic cases without requiring an additional higher-order non-linear term. Furthermore, consistent with landscape analysis and our results for planar/hyperbolic topologies, all zeroth-order transition instabilities should convert to stable first-order transitions when ψ becomes sufficiently large, provided both back-reaction and pressure remain non-zero.

Conclusions—This study investigates the spontaneous scalarization of topological AdS black holes—spherical, planar, and hyperbolic—coupled with a charged scalar field, revealing profound universal behavior. We illustrated that scalarization, a phase transition in which black holes spontaneously develop scalar hair at low temperatures, is a common feature across all three topologies.

Our study reveals that in the extended phase space, pressure universally controls the phase transitions of scalarized black holes. Increasing the pressure drives the first-order phase transition of the system to a critical point, beyond which the system enters a supercritical region. Contrarily, when we lower the pressure, the scalarization of the black holes turns into first order phase transitions with increasing phase transition temperature, which makes it more difficult to find the final stable section of solutions with very larger condensate value. This universal behavior applies to black holes with all three topologies. Furthermore, while planar and hyperbolic topologies require higher-order non-linear terms to generate unstable branches of solutions in the first-order phase transitions, the spherical topology inherently exhibits such unstable branch of solutions, requiring no additional non-linear terms.

In the previous studies, the scalarization phase transition in the low pressure region of the spherical topology case is claimed to be zeroth-order and the scalarized solutions are all unstable. However, the zeroth-order phase transition is a pathological signal that should not occur in a stable setup. From a landscape analysis and with the above universality, we claimed that the previous result of the zeroth-order phase transitions is caused by the misleading from the incomplete branch of unstable solutions, therefore, the unstable section of solutions is expected to turn back to a new branch of stable solutions with lower free energy, while the zeroth-order phase transition exhibited in spherical topology will be replaced by a first order phase transition with a very high transition temperature into the scalarized black holes.

In summary, our work investigates the phase transition behaviors of scalarized black holes from the perspective of different topologies. It establishes the universal role of pressure as a key control parameter in the extended phase space of black holes and specifically reveals the unique and rich physics of spherical topology black holes during scalarization. These findings not only deepen the understanding of gravitational nonlinearity and black hole thermodynamics, but also provide new insights for studying phase transitions in strongly coupled systems within the AdS/CFT correspondence framework.

Acknowledgements.—We are grateful to Xin Zhao for useful discussions. This work is supported by NSFC with Grant Nos. 12533001, 12575049, 12473001, 12205039, 12305058, 11965013 and 12575054. ZYN is partially supported by Yunnan High-level Talent Training Support Plan Young & Elite Talents Project (Grant No. YNWR-QNBJ-2018-181). This work is also supported by the National SKA Program of China (grant Nos. 2022SKA0110200 and 2022SKA0110203) and the 111 Project (Grant No. B16009).

* niezy@kust.edu.cn
† weishw@lzu.edu.cn
‡ zhangxin@neu.edu.cn

[1] R. Bartnik and J. Mckinnon, Phys. Rev. Lett. **61**, 141 (1988).
[2] C. A. R. Herdeiro and E. Radu, Int. J. Mod. Phys. D **24**, 1542014 (2015), arXiv:1504.08209 [gr-qc].
[3] T. Damour and G. Esposito-Farese, Phys. Rev. Lett. **70**, 2220 (1993).
[4] H. O. Silva, J. Sakstein, L. Gualtieri, T. P. Sotiriou, and E. Berti, Phys. Rev. Lett. **120**, 131104 (2018), arXiv:1711.02080 [gr-qc].
[5] D. D. Doneva and S. S. Yazadjiev, Phys. Rev. Lett. **120**, 131103 (2018), arXiv:1711.01187 [gr-qc].
[6] G. Antoniou, A. Bakopoulos, and P. Kanti, Phys. Rev. Lett. **120**, 131102 (2018), arXiv:1711.03390 [hep-th].
[7] C. A. R. Herdeiro, E. Radu, N. Sanchis-Gual, and J. A. Font, Phys. Rev. Lett. **121**, 101102 (2018), arXiv:1806.05190 [gr-qc].
[8] P. V. P. Cunha, C. A. R. Herdeiro, and E. Radu, Phys. Rev. Lett. **123**, 011101 (2019), arXiv:1904.09997 [gr-qc].
[9] C. A. R. Herdeiro, E. Radu, H. O. Silva, T. P. Sotiriou, and N. Yunes, Phys. Rev. Lett. **126**, 011103 (2021), arXiv:2009.03904 [gr-qc].
[10] E. Berti, L. G. Collodel, B. Kleihaus, and J. Kunz, Phys. Rev. Lett. **126**, 011104 (2021), arXiv:2009.03905 [gr-qc].
[11] S. Garcia-Saenz, A. Held, and J. Zhang, Phys. Rev. Lett. **127**, 131104 (2021), arXiv:2104.08049 [gr-qc].
[12] C.-Y. Zhang, Q. Chen, Y. Liu, W.-K. Luo, Y. Tian, and B. Wang, Phys. Rev. D **106**, L061501 (2022), arXiv:2204.09260 [gr-qc].
[13] J. M. Maldacena, Adv. Theor. Math. Phys. **2**, 231 (1998), arXiv:hep-th/9711200.
[14] S. A. Hartnoll, C. P. Herzog, and G. T. Horowitz, Phys. Rev. Lett. **101**, 031601 (2008), arXiv:0803.3295 [hep-th].
[15] S. A. Hartnoll, C. P. Herzog, and G. T. Horowitz, JHEP **12**, 015 (2008), arXiv:0810.1563 [hep-th].
[16] R.-G. Cai, Z.-Y. Nie, and H.-Q. Zhang, Phys. Rev. D **82**, 066007 (2010), arXiv:1007.3321 [hep-th].
[17] R.-G. Cai, Z.-Y. Nie, and H.-Q. Zhang, Phys. Rev. D **83**, 066013 (2011), arXiv:1012.5559 [hep-th].
[18] H.-F. Li, R.-G. Cai, and H.-Q. Zhang, JHEP **04**, 028 (2011), arXiv:1103.2833 [hep-th].
[19] R.-G. Cai, L. Li, and L.-F. Li, JHEP **01**, 032 (2014), arXiv:1309.4877 [hep-th].
[20] R.-G. Cai, L. Li, L.-F. Li, and R.-Q. Yang, Sci. China Phys. Mech. Astron. **58**, 060401 (2015), arXiv:1502.00437 [hep-th].
[21] D. Kubiznak and R. B. Mann, JHEP **07**, 033 (2012), arXiv:1205.0559 [hep-th].
[22] S. Gunasekaran, R. B. Mann, and D. Kubiznak, JHEP **11**, 110 (2012), arXiv:1208.6251 [hep-th].
[23] R.-G. Cai, L.-M. Cao, L. Li, and R.-Q. Yang, JHEP **09**, 005 (2013), arXiv:1306.6233 [gr-qc].
[24] S.-W. Wei and Y.-X. Liu, Phys. Rev. Lett. **115**, 111302 (2015), [Erratum: Phys.Rev.Lett. 116, 169903 (2016)], arXiv:1502.00386 [gr-qc].
[25] S.-W. Wei, Y.-X. Liu, and R. B. Mann, Phys. Rev. Lett. **129**, 191101 (2022), arXiv:2208.01932 [gr-qc].
[26] Z.-Q. Zhao, Z.-Y. Nie, J.-F. Zhang, and X. Zhang, Chin. Phys. Lett. **42**, 101102 (2025), arXiv:2504.04995 [gr-qc].
[27] G. Guo, P. Wang, H. Wu, and H. Yang, Eur. Phys. J. C **81**, 864 (2021), arXiv:2102.04015 [gr-qc].
[28] G. Guo, P. Wang, H. Wu, and H. Yang, Phys. Rev. D **105**, 064069 (2022), arXiv:2107.04467 [gr-qc].
[29] Z.-Q. Zhao, X.-K. Zhang, and Z.-Y. Nie, JHEP **02**, 023 (2023), arXiv:2211.14762 [hep-th].
[30] X.-K. Zhang, C.-Y. Xia, Z.-Y. Nie, and H. Zeng, Phys. Rev. D **105**, 046016 (2022), arXiv:2105.14294 [hep-th].
[31] Z.-Q. Zhao, Z.-Y. Nie, J.-F. Zhang, and X. Zhang, Eur. Phys. J. C **85**, 1064 (2025), arXiv:2506.17274 [hep-ph].